Inorganic Chemistry

ARTICLE

pubs.acs.org/IC

Synthesis, Characterization, and Electronic Structure of New Type of Heterometallic Boride Clusters

Shubhankar Kumar Bose,[†] K. Geetharani,[†] Satyanarayan Sahoo,[†] K. Hari Krishna Reddy,[‡] Babu Varghese,[∥] Eluvathingal D. Jemmis,[‡,§] and Sundargopal Ghosh*[,†]

[†]Department of Chemistry, Indian Institute of Technology Madras, Chennai 600 036, India

[‡]Department of Inorganic and Physical Chemistry, Indian Institute of Science, Bangalore 560 022, India

[§]Indian Institute of Science Education and Research Thiruvananthapuram, CET Campus, Thiruvananthapuram, Kerala 695 016, India

[∥]Sophisticated Analytical Instruments Facility, Indian Institute of Technology Madras, Chennai 600 036, India

Supporting Information

ABSTRACT:

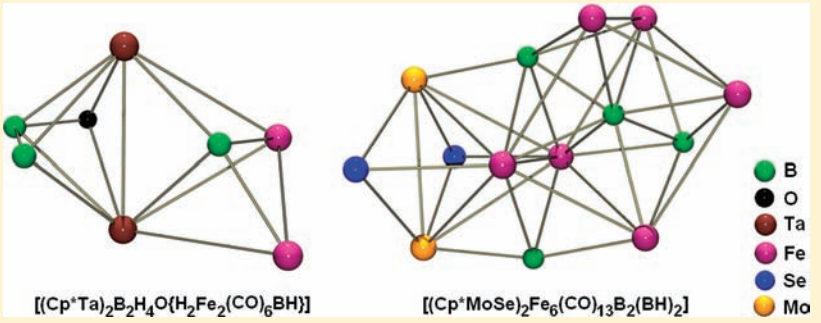

The reaction of $[Cp^*TaCl_4]$, **1** ($Cp^* = \eta^5$-C_5Me_5), with $[LiBH_4 \cdot THF]$ at −78 °C, followed by thermolysis in the presence of excess $[BH_3 \cdot THF]$, results in the formation of the oxatantalaborane cluster $[(Cp^*Ta)_2B_4H_{10}O]$, **2** in moderate yield. Compound **2** is a notable example of an oxatantalaborane cluster where oxygen is contiguously bound to both the metal and boron. Upon availability of **2**, a room temperature reaction was performed with $[Fe_2(CO)_9]$, which led to the isolation of $[(Cp^*Ta)_2B_2H_4O\{H_2Fe_2(CO)_6BH\}]$, **3**. Compound **3** is an unusual heterometallic boride cluster in which the $[Ta_2Fe_2]$ atoms define a butterfly framework with one boron atom lying in a semi-interstitial position. Likewise, the diselenamolybdaborane, $[(Cp^*Mo)_2B_4H_4Se_2]$, **4** was treated with an excess of $[Fe_2(CO)_9]$ to afford the heterometallic boride cluster $[(Cp^*MoSe)_2Fe_6(CO)_{13}B_2(BH)_2]$, **5**. The cluster core of **5** consists of a cubane $[Mo_2Se_2Fe_2B_2]$ and a tricapped trigonal prism $[Fe_6B_3]$ fused together with four atoms held in common between the two subclusters. In the tricapped trigonal prism subunit, one of the boron atoms is completely encapsulated and bonded to six iron and two boron atoms. Compounds **2**, **3**, and **5** have been characterized by mass spectrometry, IR, ^1H, ^{11}B, ^{13}C NMR spectroscopy, and the geometric structures were unequivocally established by crystallographic analysis. The density functional theory calculations yielded geometries that are in close agreement with the observed structures. Furthermore, the calculated ^{11}B NMR chemical shifts also support the structural characterization of the compounds. Natural bond order analysis and Wiberg bond indices are used to gain insight into the bonding patterns of the observed geometries of **2**, **3**, and **5**.

INTRODUCTION

The classic development of this subarea of chemistry begins with the finding of a new compound type and proceeds through synthetic improvements and structural development to systematic examination of reactivity. Although for the past 25 years Fehlner and others have worked on boron-transition metal clusters,[1−6] development in this area has been slow, partly due to the lack of convenient high-yield synthetic methods.[7] Only the most stable/least reactive compounds are characterized significantly restricting the scope of the chemistry particularly when early transition metals are of interest. However, due to the recent availability of convenient routes to metallaboranes,[8] the development of synthetic chemistry has permitted a focus on reactivity.

After it had been revealed that the reaction of $[(Cp^*M)_2B_4H_8]$ (M = Re and Ru) with monoborane reagents led to the isolation of higher nuclearity *closo*-rhenaboranes[9] and hydrogen-rich *nido*-ruthenaboranes,[10] reinvestigation of an allied tantalum system became of interest. Although the objective of generating higher nuclearity clusters was not achieved, one interesting oxatantalaborane $[(Cp^*Ta)_2B_4H_{10}O]$ **2** was isolated. Up until now, only few structurally characterized oxametallaboranes were known.[11−16] Transition metal carbonyl compounds, for example, $Fe_2(CO)_9$ or $Co_2(CO)_8$, have received considerable attention in metallaborane

Received: May 18, 2011
Published: August 29, 2011

ACS Publications © 2011 American Chemical Society

Scheme 1. Synthesis of 2 and 3

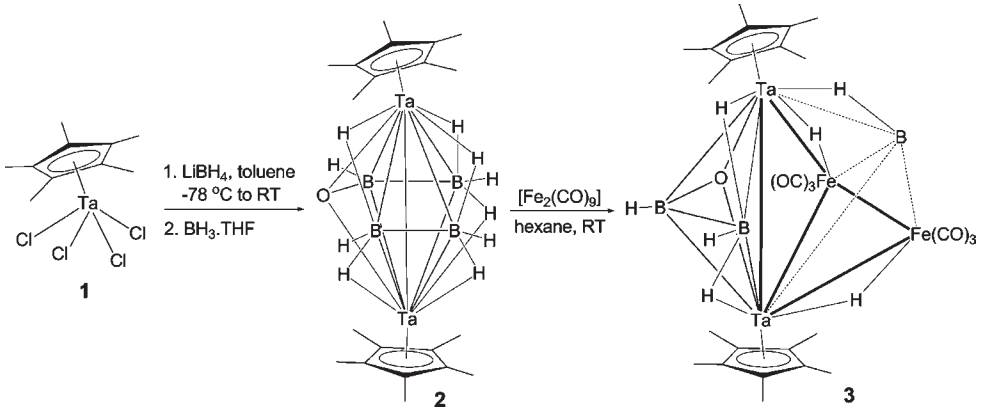

chemistry in connection with their potential as versatile reagents in metal cluster building reactions. Therefore, upon the availability of **2**, the chemistry was elaborated by means of a cluster expansion reaction with $[Co_2(CO)_8]$, which led to decomposition, whereas reaction with $[Fe_2(CO)_9]$ in hexane led to the isolation of an unusual boride cluster, $[(Cp^*Ta)_2B_2H_4O\{H_2Fe_2(CO)_6BH\}]$ **3**. Extension of this approach to the diselenamolybdaborane, $[(Cp^*Mo)_2B_4H_4Se_2]$[17] **4**, resulted in the formation of the heterometallic boride cluster $[(Cp^*MoSe)_2Fe_6(CO)_{13}B_2(BH)_2]$ **5**. Reported here are the synthesis, structural characterization, and bonding of these seven-, eight-, and fourteen-vertex clusters. In addition, to provide some insight into the nature of bonding in clusters **2**, **3**, and **5**, in particular the short Ta−Ta bond distance, density functional theory (DFT) studies were carried out.

RESULTS AND DISCUSSION

Formation and Properties of 2. Recently, the in situ generated intermediate, produced in the reaction of $[Cp^*TaCl_4]$ **1** with $[LiBH_4\cdot THF]$, provided a series of tantalaborane clusters by thermolysis with monoborane reagents.[18] An unidentified compound, oxatantalaborane **2**, has been isolated and characterized in the present study (Scheme 1). It was obtained in 16% yield by the thermolysis in toluene at 110 °C for two days. The mass spectrum of **2** shows a molecular ion at m/z = 701 corroborating the composition of $C_{20}H_{40}Ta_2B_4O$. The ^{11}B NMR spectrum indicates four distinct boron environments with an intensity ratio of 1:1:1:1. Besides four types of BH terminal protons, the ^1H NMR spectrum of **2** shows one kind of Cp* and three types of Ta−H−B environments with equal intensity. The variable temperature $^1H\{^{11}B\}$ and $^{11}B\{^1H\}$ NMR study revealed no fluxional behavior associated with Ta−H−B or B−H bonding.

The framework structure of **2** became clear when a solid state structure was determined. The single crystal X-ray structure of **2**, shown in Figure 1, clearly shows that one oxygen atom is bound to two Ta metals and one boron atom. Compound **2** can be considered as an edge fused cluster in which a trigonal bipyramidal unit $[Ta_2B_2O]$ has been fused with a tetrahedral core $[Ta_2B_2]$ by means of a common $[Ta_2]$ edge. Although we do not have any direct evidence for the source of oxygen in the generation of **2**, it has previously been observed in other polyborane/$[\{Cp^*RhCl_2\}_2]$ systems when handled in air.[12,19] Thus, the source of the oxygen atom leading to the formation of **2** is probably trace amounts of water/air bound to the silica gel. The oxygen atom in **2** is disordered over two positions, and the disorder has been modeled over two sites, each with 50% occupancy. The Ta1−Ta2 bond length of 2.7554(2) Å is significantly shorter than that observed in $[(Cp^*Ta)_2(B_2H_6)_2]$ (2.9325(4) Å)[18b] and other tantalaborane clusters.[18a] The significant shortening of the Ta−Ta bond might arise from the effect of the oxygen atom, which withdraws electron density from the cluster. The boron−oxygen bond length is found to be 1.548(10) Å, which is comparable with the other oxametallaboranes, for example, 1.523 Å in $[9,9\text{-}(PMe_2Ph)_2\text{-}arachno\text{-}9,6\text{-}PtOB_8H_{10}]$[14] and 1.521 Å in $[7\text{-}(Cp^*)\text{-}10\text{-}(NEt_3)\text{-}nido\text{-}7,12\text{-}RhOB_{10}H_{10}]$.[12] In **2**, all the Ta−H−B hydrogen atoms were not located; however, they were confirmed by the low-temperature $^1H\{^{11}B\}$ NMR spectrum.

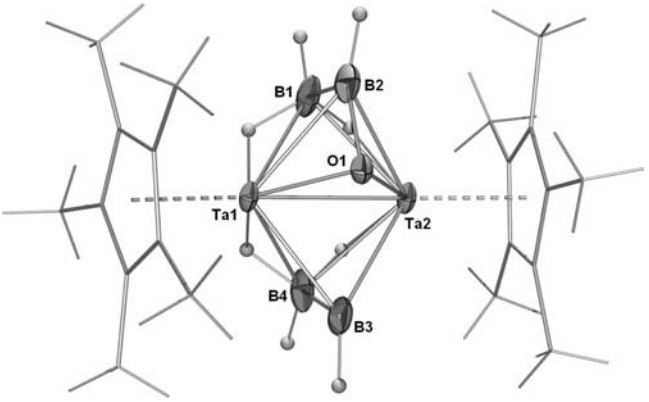

Figure 1. Molecular structure and labeling diagram for **2**. Thermal ellipsoids are shown at the 30% probability level. Selected bond lengths (Å) and angles (deg): Ta1−Ta2 2.7554(2), Ta1−B1 2.387(6), Ta1−B2 2.419(7), Ta1−B3 2.416(7), Ta1−B4 2.389(7), Ta1−O1 2.050(6), B1−B2 1.750(11), B3−B4 1.736(11), and B2−O1 1.548(10); B2−B1−Ta1 69.6(3), O1−B2−B1 112.2(6), Ta2−B1−Ta1 70.59(19), and Ta1−O1−Ta2 83.6(2).

The ^1H and ^{11}B NMR spectra are consistent with the solid state structure of **2**. The ^{11}B NMR spectrum exhibits four resonances at δ 23.9, −0.8, −4.3, and −34.1 ppm. The ^1H NMR spectrum of **2** is somewhat unusual, but it was unraveled with a $^1H\{^{11}B\}/^{11}B\{^1H\}$ HSQC experiment. The HSQC spectrum

dx.doi.org/10.1021/ic201046g |*Inorg. Chem.* 2011, 50, 9414–9422

Table 1. Selected Structural Parameters and Chemical Shifts (^{1}H and ^{11}B NMR) of Tetrametal Boride Clusters (Cp = η^5-C_5H_5)

compd	d B from M_w–M_w axis [Å][a]	dihedral angle [deg][b]	^{1}H NMR[ppm] [M–H–B] expt[c]	^{1}H NMR[ppm] [M–H–B] calc[d]	^{11}B NMR [ppm] expt[c]	^{11}B NMR [ppm] calc[d]	ref
$[HFe_4(CO)_{12}BH_2]$	0.3	114	−11.9	−19	106	110.3	24
$[HRu_4(CO)_{12}BH_2]$	0.29	118	−8.5	−13	113	92.5	28a
$[H_2Cp^*RhRu_3(CO)_8(PPh_3)BH]$	0.15	109	−4.9	−8	149	150.5	23
$[HCp^*IrRu_3(CO)_{10}BH_2]$[e]	0.35	93	−6.0, −6.4	−12	92.7	96.3	23
$[HCpW(CO)_2Ru_3(CO)_9BH]$	0.28	111	−6.6	−12	131.9	113.8	28b
$[(Cp^*Ta)_2B_2H_4O\{H_2Fe_2(CO)_6BH\}]$ **3**	0.24	108	−2.5	−9	153	143.2	this work

[a] The distance of the boron atom from the line connecting the wing-tip metal atoms. [b] Dihedral angle between the butterfly wings. [c] Experimental value. [d] Calculated values are part of the current paper. [e] Given values for one isomer.

evidently shows that three of the ^{11}B resonances, appearing at δ 23.9, −4.3, and −34.1 ppm, are associated to three hydrogen atoms (one B–H and two Ta–H–B), whereas the resonance at δ −0.8 ppm is only linked to one hydrogen atom (see Figure S1 in the Supporting Information). Consistent with this structural conclusion, the resonance at δ −0.8 ppm has been attributed to the boron, which is connected to the oxygen atom. The IR spectrum of **2** shows one broad peak at 1380 cm^{-1}, which has been assigned to the B–O stretches.

Synthesis and Characterization of Boride Clusters 3 and 5. Cluster expansion reactions are now well-known;[20,21] however, examples proceeding in high yield with clean and well-defined stochiometry are scarce. The metallaheteroboranes **2** and **4** consist of an M_2B_4 core having one and two group-16 elements, respectively. The oxatantalaborane **2** undergoes a clean cluster-building reaction with $[Fe_2(CO)_9]$ in hexane at room temperature to generate a single boride cluster **3** by the loss of one boron from the species in solution (as monitored by ^{11}B NMR; Scheme 1), whereas mild thermolysis of **4** with excess of $[Fe_2(CO)_9]$ in hexane for 4 h yielded the heterometallic boride cluster **5** in parallel with the formation of the cubane-type cluster $[(Cp^*Mo)_2(\mu_3\text{-}Se)_2B_2H(\mu\text{-}H)\{Fe(CO)_2\}_2Fe(CO)_3]$.[22] Clusters **3** and **5** were air-stable reddish brown solids, isolated by preparative thin-layer chromatography (TLC) in 58% and 8% yield, respectively. Compounds **3** and **5** have been characterized spectroscopically as well as by single crystal X-ray diffraction analysis.

The FAB mass spectrum of **3** gave a molecular ion peak at m/z = 967, corresponding to $C_{26}H_{37}B_3O_7Fe_2Ta_2$, while the IR spectrum displayed intense bands at 1946, 1978, and 2031 cm^{-1}, characteristic of terminal carbonyl groups and a band at 2464 cm^{-1} due to the terminal B–H stretches. The ^{11}B NMR spectrum displays three resonances with an equal intensity, distributed over an unusually large chemical shift range of ca.160 ppm. One of the resonances at δ 153 ppm is significantly downfield shifted relative to the starting material **2** (δ 23.9 ppm), implying a greater degree of boron–metal interactions. The observed ^{11}B NMR shift of the boride cluster appears to depend only on the number of direct M–B interactions; however, the ^{11}B NMR chemical shift of **3** is not very consistent with other structurally characterized M_4B clusters, except the $[H_2Cp^*RhRu_3(CO)_8(PPh_3)BH]$[23] cluster (Table 1). This inaptness may be due to the differing character of the metals and ligands.

The solid state X-ray structure of **3**, shown in Figure 2, confirms the structural inferences made on the basis of spectroscopic results. The molecular structure of **3** represents a novel

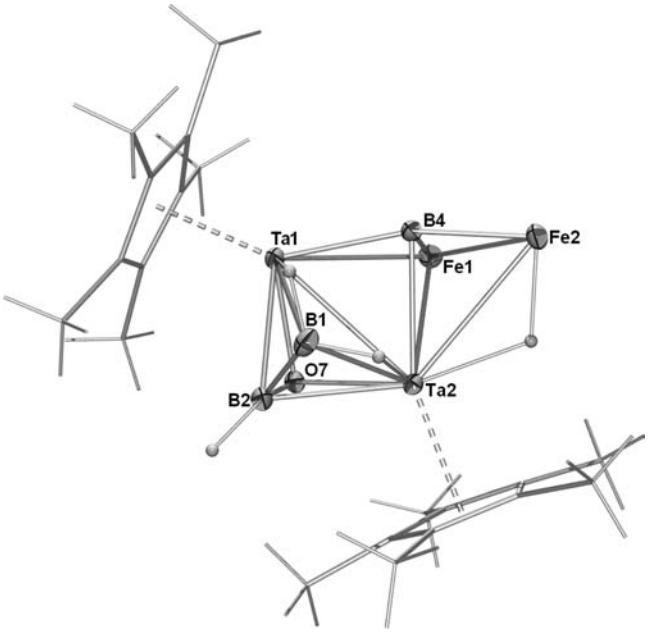

Figure 2. Molecular structure and labeling diagram for **3** (terminal CO ligands omitted for clarity). Thermal ellipsoids are shown at the 30% probability level. Selected bond lengths (Å) and angles (deg): Ta1–Ta2 2.9142(6), Ta1–Fe1 3.0262(15), Ta2–Fe2 2.9607(14), Fe1–Fe2 2.7201(13), Ta1–O7 2.075(4), Ta1–B1 2.380(6), B1–B2 1.712(10), B2–O7 1.429(8), Ta1–B4 2.172(6), Ta2–B4 2.367(6), and Fe1–B4 2.038(7); Ta2–B1–Ta1 75.37(19), Ta1–O7–Ta2 88.58(14), Ta1–B4–Ta2 79.8(2), Fe1–B4–Fe2 86.4(3), Ta1–B4–Fe2 166.1(3), and Ta2–B4–Fe2 86.4(2).

class of edge fused clusters in which a trigonal bipyramidal fragment $[Ta_2B_2O]$ has been fused with a capped butterfly core $[Ta_2Fe_2B]$ via a common $[Ta_2]$ edge. Alternatively, as shown in Figure 2, cluster **3** can also be viewed as an edge fused cluster in which the Ta1–Fe1–Fe2–B4 fragment represents the butterfly core with a Ta2 atom residing midway between Ta1 and Fe2. In **3**, the unique boron atom (B4) lies 0.2408 Å above the Ta_{wing}–Fe_{wing} (i.e., Ta1–Fe2) axis. The internal dihedral angle of the Ta_2Fe_2 butterfly is 108°, which corresponds well with the values observed for $[H_2Cp^*RhRu_3(CO)_8(PPh_3)BH]$ (109°),[23] $[HFe_4(CO)_{12}BH_2]$ (114°)[24], and for a four-atom butterfly cluster (109°) derived from an octahedron (Table 1).[25] Although the Fe–Fe bond distance of 2.7201(13) Å falls in the range associated with a M–M single bond,[26] the Ta–Ta bond distance

dx.doi.org/10.1021/ic201046g |Inorg. Chem. 2011, 50, 9414–9422

Scheme 2. Synthesis of 5 and the Cubane-Type Cluster $[(Cp^*Mo)_2(\mu_3\text{-}Se)_2B_2H(\mu\text{-}H)\{Fe(CO)_2\}_2Fe(CO)_3]$

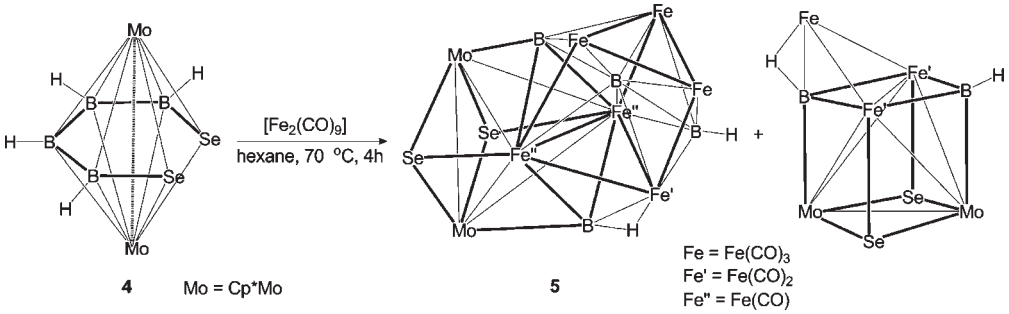

of 2.9142(6) Å is significantly longer than that of **2**. This variation of bond length might be due to the heterometallic boride core $[Ta_2Fe_2B]$, which perturbs the electronic structure of the metal cage. Butterfly boride clusters now have been fully characterized;[27] however, as yet, there are only a few examples known that incorporate heterometallic cages containing a single boron atom.[23,28] Similar to **2**, compound **3** also exhibits an oxygen-to-cluster connectivity three. The boron−oxygen bond length of 1.429(8) Å is significantly shorter in comparison to those observed in **2** and other oxametallaborane clusters.[12−16] Although all of the terminal and bridging hydrogen atoms were not located in the X-ray diffraction study, evidence for their presence has been supported by the $^1H\{^{11}B\}$ NMR spectrum.

Solution Properties of 3. In a $[D_8]$-toluene solution, the room-temperature $^1H\{^{11}B\}$ NMR spectrum exhibits two resonances due to the Cp* protons at δ 2.03 and 1.84 ppm, indicating two different Ta environments. In addition to the resonances due to BH terminal protons, the ^1H NMR spectrum reveals three broad resonances at δ −2.89, −4.12, and −7.93 and two sharp signals at δ −13.85 and −16.54 ppm. The latter resonances are typically arising from a M−H−M (M = Fe, Ru, Rh, or Ir) bridging hydride.[23,24,28] The resonances at δ −4.12 and −7.93 ppm are assigned to two Ta−H−B bridging hydrogens of the trigonal bipyramidal core, $[Cp^*_2Ta_2B_2O]$. However, the resonance at δ −2.89 ppm has been assigned to the hydrogen atom that is bridged between B4 and Ta1 atoms (Figure 2). In a further attempt to confirm these assignments, a 2D $^1H\{^{11}B\}/^{11}B\{^1H\}$ HSQC experiment was performed, which is consistent with the proposed structure of **3**, shown in Scheme 1. Variable temperature $^1H\{^{11}B\}$ NMR spectra of **3** demonstrate that Ta−H−Fe protons in the Ta_2Fe_2B butterfly core exchange rapidly on the NMR time scale at a temperature of 85 °C or above (see Figure S2 in the Supporting Information).

Characterization of $[(Cp^*MoSe)_2Fe_6(CO)_{13}B_2(BH)_2]$, 5. The identity of the heterometallic boride cluster **5**, isolated from the reaction of **4** with $[Fe_2(CO)_9]$ (Scheme 2), was not readily elucidated without the aid of crystal structure determination. The molecular structure of the boride cluster is shown in Figure 3. The central core of **5** can be regarded as a facially fused cluster, which consists of a cubane and tricapped trigonal prism (ttp) subunit. A group of six iron atoms form an idealized trigonal prism with an encapsulated boron atom of which two rectangular and one triangular face is capped by boron atoms B2, B3, and B4, respectively. The trigonal prism framework is not unusual in boride chemistry and was found previously in $[N(PPh_3)_2][Ru_6H_2(CO)_{18}B]$[29] and $[AsPh_4]_2[HFe_7(CO)_{20}B]$.[26] However, the boron centered fused cubane-trigonal prismatic structure of **5** appears

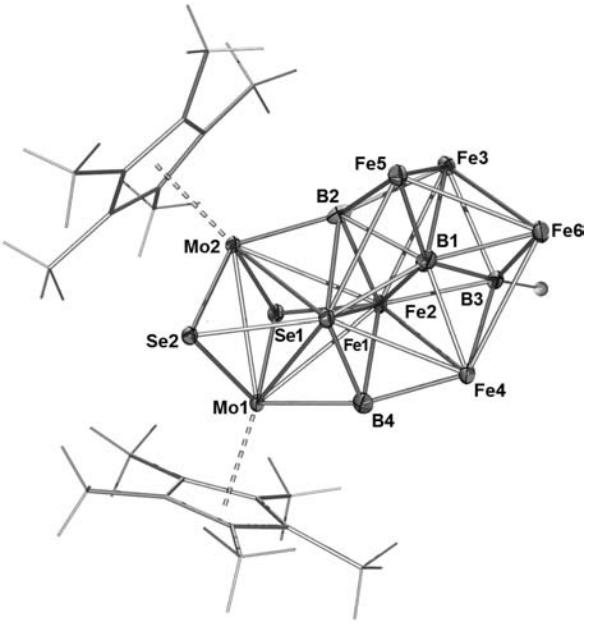

Figure 3. Molecular structure and labeling diagram for **5** (terminal CO ligands omitted for clarity). Thermal ellipsoids are shown at the 30% probability level. Selected bond lengths (Å) and angles (deg): Mo1−Mo2 2.8645(8), Mo1−Se1 2.4434(8), Mo2−B2 2.126(8), Fe1−Se2 2.3665(11), Fe1−B2 2.089(7), Fe2−B4 2.088(7), Fe1−Fe2 2.5022(13), Fe1−Fe4 2.6392(13), Fe3−Fe5 2.7044(13), Fe5−Fe6 2.6827(13), B1−B2 1.765(11), B1−B3 1.827(12), B1−Fe1 2.038(8), and B1−Fe3 2.109(8); Mo1−Mo2−Fe2 60.16(2), Mo1−Fe1−Fe2 64.67(3), Mo2−B2−Fe5 143.0(4), Fe2−B1−Fe6 135.2(4), and B2−B1−B3 118.9(5).

to be the first cluster of its type, not only with respect to the environment of the boron atom but also with respect to the metal framework.

The boron atom (B1) lies at the center of a trigonal prismatic cage, bonded to six Fe atoms and two boron atoms (B2 and B3). Shorter Fe−Fe distances are observed between the trigonal atoms; they are in the range of 2.5031−2.7043 Å, comparable to the sum of the van der Waals radii for metallic iron (2.52 Å), while the lengths (Fe1−Fe5, Fe2−Fe3, Fe4−Fe6) are on average 2.8082 Å. The three boron atoms displaced toward each other such that the B1−B2 and B1−B3 separation is 1.765(11) and 1.827(12) Å, respectively. This value lies within the range observed for boron−boron distances in $[Rh_3Ru_6(CO)_{23}B_2]$ (1.80(2) Å) and $[Co_5(CO)_{14}B(BH)]$ (1.85(4) Å).[30,31] The Fe−B1 distances

dx.doi.org/10.1021/ic201046g |Inorg. Chem. 2011, 50, 9414–9422

Chart 1. Different Types of Transition Metal Boride Clusters

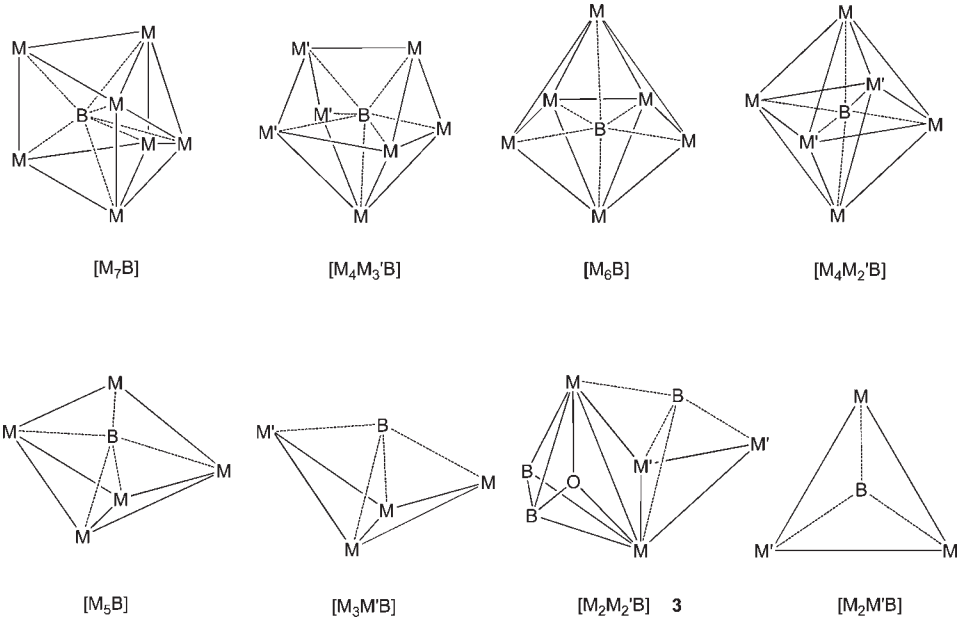

for the six iron atoms making up the trigonal prism are within the normal range expected. However, the boron atom (B1) is not symmetrically located in the trigonal prism, being somewhat closer to Fe1 and Fe5 than the other four iron atoms (average 2.042 vs 2.091 Å).

In complex **5**, another subunit consists of a distorted $Mo_2Fe_2Se_2B_2$ cubane core. Alternatively, the core structure can be viewed as a Mo_2Fe_2 tetrahedron face capped by two selenium and two boron atoms. In this complex, the Mo−Mo bond, bridged by two selenium atoms, has the bond length of 2.8645(8) Å, which is similar to that of the Mo−Mo bond in $[Cp_2Mo_2(\mu_3\text{-}S)_4Ni_2(CO)_2]$.[32] The Mo−Fe1 distances (2.76 and 2.79 Å) are consistent with the existence of a single bond, being somewhat shorter than the corresponding distances in $[Cp_2Mo_2FeTe_2(CO)_7]$[33] (2.84 Å) and being similar in length to that found in $[FeCo_2MoSAsMe_2Cp(CO)_8]$.[34] The Fe−Se distances (2.3665(11) and 2.3977(11) Å) are slightly longer than the iron−selenium cubane cluster $[(CpFe)_4Se_4](PF_6)_3$ (2.3305 Å).[35] The average bond length of Mo−Se is 2.4302 Å, 0.14 Å longer than that observed in the cubane-like compound $[MoAg_3Se_3Br]$.[36]

The ^1H and ^{11}B NMR spectra are consistent with the solid-state X-ray structure of **5**, which rationalizes the presence of four ^{11}B resonances at δ 162.5, 158.2, 106.2, and 67.8 ppm (1:1:1:1). The ^1H NMR spectra showed one broad signal at the lower field for the terminal BH proton, two sets of distinct chemical shift for the two Cp* ligands, and a singlet at the higher field for the Fe−H−B proton at δ −15.65 ppm. The ^{77}Se NMR spectra display two sets of resonance frequencies due to two chemically inequivalent selenium nuclei. The mass spectrum shows, in addition to the molecular-ion peak at m/z = 1364 corroborating the composition of $C_{33}H_{32}B_4Fe_6Mo_2O_{13}Se_2$, thirteen major peaks for the loss of CO ligands.

The position of the boron resonance for B1 (δ 106.2 ppm) calls for some comment, while the chemical shift values for ^{11}B NMR spectral resonances are sensitive to the environment, with interstitial atoms being characterized by unusually low field chemical shifts and a sharp signal. Although B1 is directly bonded to six iron atoms, as indeed it is in the interstitial position of the boride cluster, its resonance appears upfield from the expected chemical shift for the encapsulated boron atom.[26] The change in connectivity associated with B1 is that it is also directly linked to two boron atoms rather than fully connected to the metal atoms. The two resonances of relative intensity 1:1 at δ 162.5 and 158.2 ppm can be assigned to the four and six connected boron atoms B4 and B2, respectively. The resonance at δ 67.8 ppm can be ascribed to the square face capped five connectivity boron nucleus (B3) as it became a doublet in the proton coupled ^{11}B spectrum.

The bonding of **2** can be considered from the *mno* electron counting rule.[37] The number of skeletal electron pairs required for this structure is *m* (number of individual polyhedral fragments) + *n* (number of vertexes in the polyhedron) + *o* (number of single vertex sharing junctions) + *p* (number of missing vertexes in the idealized *closo* skeleton). Here, m = 3, n = 17, o = 2, and p = 4. Thus, according to this rule, **2** needs 26 skeletal electron pairs for the cluster bonding. The total number of electron pairs available in **2** is 28 [2 × Cp* (30e) + 4 × BH (8e) + 6 × μH (6e) + 1 × O (2e) + 2 × Ta (10e) = 56e, i.e., 28 electron pairs]. The two Ta atoms are bonded by a double bond, which is identified after analyzing the MOs of **2**. Therefore, the subtraction of two electron pairs corresponding to the Ta−Ta double bond leads to the 26 available electron pairs for skeletal bonding.

Geometric and Spectroscopic Comparison of Boride Clusters. Metallaboranes are predominantly exemplified by boron-rich clusters rather than metal-rich clusters.[27] The characteristical feature that separates the boride clusters (metal-rich metallaboranes)[24,27] from the metallaboranes is the greater number of boron-to-metal bonding contacts at the expense of boron−hydrogen bonds. The common range of metal skeletons are shown in Chart 1.[38−42] Metal frameworks that are represented include the M_4 butterfly, the M_5 square-based pyramid, the M_6 octahedron, the M_6 trigonal prism, and the M_7 capped trigonal prism together with a variety of more unusual geometries.

dx.doi.org/10.1021/ic201046g |*Inorg. Chem.* 2011, 50, 9414–9422

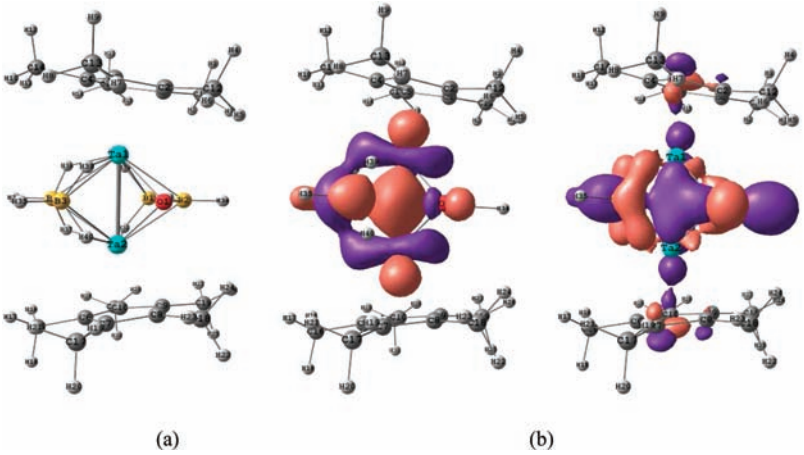

Figure 4. (a) DFT optimized structure of **2**. (b) MOs corresponding to the Ta−Ta double bond in compound **2**.

■ COMPUTATIONAL STUDIES

NMR Chemical Shifts. The effectiveness of DFT at handling NMR calculations on ^{11}B NMR chemical shifts has been demonstrated by studies on many boranes and heteroboranes.[43,44] The accuracy has been sufficient to resolve a number of outstanding problems in the field. In the case of metal-rich metallaborane, it is still a challenge, particularly for the heavier transition metals such as Ta. In addition, the presence or absence of bridging hydrogen atoms, the number of direct metal−boron bonds, the metal identity, and coordination number are all important in determining the boron chemical shifts.[45]

The isotropic NMR chemical shifts were calculated using DFT methods to validate the experimental results. All electrons in the EPR-II basis set of H, B, C, and O atoms and LANL2DZ basis set of transition metals have been used. The NMR data for **3** and other boride clusters are listed and compared in Table 1, where it can be seen that there is good agreement between the observed and the calculated ^{11}B NMR chemical shifts.

Structural Analysis. Geometry optimizations are performed on structures **2**, **3**, and **5** using DFT theory, and the parameters are in good agreement with the experimental data. Structure **2** is a typical metallaborane, and it is also shown to obey electron counting rules. In structure **2**, there is a Ta−Ta double bond; a σ bond involving the d_z^2 orbital and a π bond involving the d_{yz} orbital of the metals (Figure 4). Structures of compounds **3** and **5** are complicated; thus, applying the electron counting rules is not possible. Therefore, Wiberg bond indices (WBI)[46] have been used to understand the metal−metal interaction in compounds **3** and **5**. The interesting structural feature of **3** is the Ta_2Fe_2B butterfly framework (Figure 5). Using NBO[47] and WBI, we have analyzed the metal−metal and metal−boron bonding in the butterfly unit, which is shown in Figure 5b.

In **3**, the Ta−Ta bond is weakened and elongated with respect to that in **2**. The single bond involving the d_z^2 orbital of tantalum atoms remains the same as in **2**. However, the d_{yz} orbital is engaged in bonding with the Fe atoms, and hence, the Ta−Ta π bonding is absent in **3**, thus making the Ta1−Ta2 bond longer than that in **2**. In addition, the WBI also reveals that the Ta2−Fe1 bond is stronger than Ta1−Fe1 and Ta2−Fe2 (see Table S1 in the Supporting Information). As shown in Figure 5c, the B3 atom is more strongly bonded to Ta1 and Fe2 than to Ta2 and Fe1. This is due to the fact that Ta1 and Fe2 are oriented along the

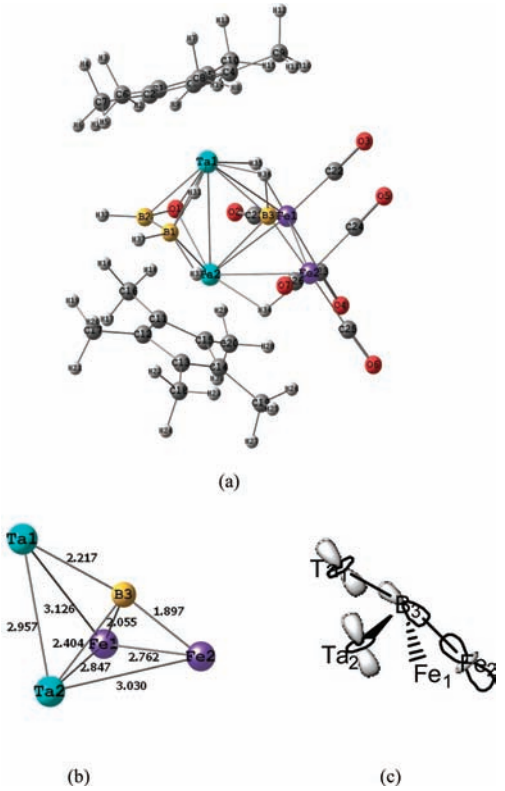

Figure 5. (a) DFT optimized structure of **3**. (b) Ta_2Fe_2B butterfly fragment in **3**. (c) The MO schematic shows strong bonding between B3−Ta1 and B3−Fe2 in **3**.

P_z axis of B3, and the p_z orbital has better overlap with the d_z^2 orbitals of the metals. The d_z^2 orbitals on Ta1 and Ta2 form a delocalized bond involving the p_z orbital on boron.

Compound **5** is a four atom face shared macropolyhedral structure formed by Fe_6B_3 and $Mo_2Se_2Fe_2B_2$ subunits with an Fe_2B_2 face shared between the two units (Figure 6). In this metal-rich boride structure, the Fe_6B_3 fragment (Figure 6b) resembles a building block of a AlB_2-type solid[48] (Figure 6c) but with only two 4-membered faces of the prism capped by the boron atoms. The bonding in AlB_2-type solids is studied, and the band structure is understood quite well.[49] The well established bonding

dx.doi.org/10.1021/ic201046g |*Inorg. Chem.* 2011, 50, 9414–9422

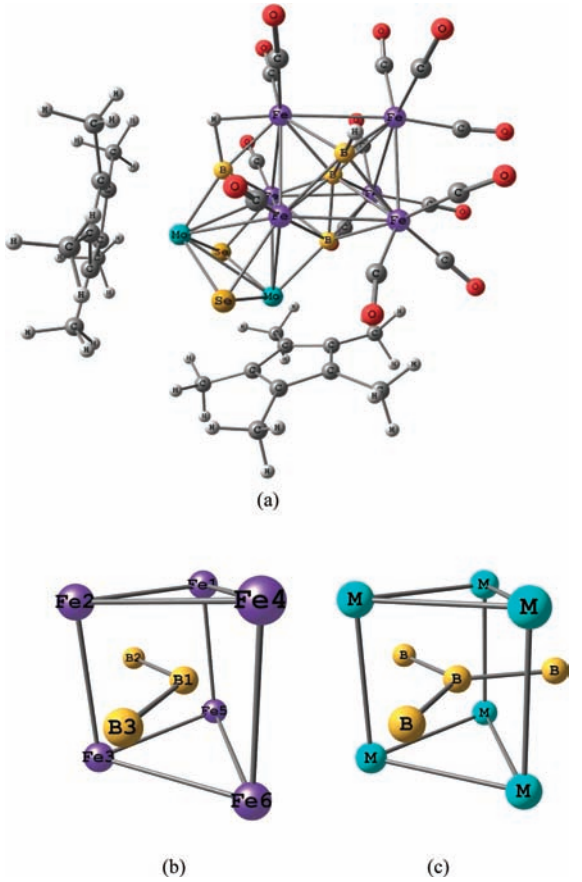

Figure 6. (a) DFT optimized structure of **5**. (b) Fe_6B_3 fragment in structure **5**. (c) Building block of AlB_2-type boride solid.

model of AlB_2 and MgB_2 solids is a mixture of in-plane B−B strong σ-covalent bonding and the M−B weak π bonding. In the case of compound **5**, a heterometallic boride, B1 is encapsulated in the interstitial hole of the Fe_6 trigonal prism. The average Fe−B1 distance 2.1 Å is slightly longer than the sum of the covalent radii of Fe (1.16 Å) and B (0.81 Å) indicating that there is no strain in the structure. The B1−B2 (1.786 Å) and B1−B3 (1.732 Å) distances are similar to the in-plane B−B distance in AlB_2 (1.737 Å) and MgB_2 (1.781 Å). Since the bonding in compound **5** is delocalized cluster bonding, it is difficult to quantify it into σ and π modes. Here, using the Wiberg bond index analysis (see Table S2 in the Supporting Information), we made an attempt to quantify the B−B and Fe−B bond strengths. The values of Wiberg bond index total, which roughly resembles the number of covalent bonds each atom forms are B1 (3.99), B2 (3.75), and B3 (3.86). For B1 the bonds with B2 and B3 corresponds to 1.66 WBI, and 1.06 WBI corresponds to the Fe−B bonds. This indicates a stronger B−B bonding and a weak Fe−B bond similar to the case in a typical AlB_2-type solid.

CONCLUSION

Metal−metal bonded dinuclear complexes of early transition metals exhibit a rich and diverse chemistry.[50] In this Article, we have described the synthesis and characterization of a new type of heterometallic boride cluster **3** derived from **2** and $[Fe_2(CO)_9]$. Clusters **2** and **3** have their oxygen atom in the open face and exhibit an oxygen-to-cluster connectivity three. The structure of cluster **5** is unique both as far as the environment of the boron atoms and the geometry of the metal skeleton are concerned. Computational studies support the structures that are characterized. The metal−metal bonding and the novel metal−boron bonding are analyzed using NBO analysis and WBI analysis. The transition from metallaborane to discrete metal boride clusters is being made, and there should now follow a wealth of new and exciting chemistry.

EXPERIMENTAL SECTION

General Procedures and Instrumentation. All the operations were conducted under an Ar/N_2 atmosphere using standard Schlenk techniques or a glovebox. Solvents were distilled prior to use under Argon. $[Cp^*TaCl_4]$, $[BH_3\cdot THF]$, $[LiBH_4\cdot THF]$, and $[Fe_2(CO)_9]$ (Aldrich) were used as received. $[(Cp^*Mo)_2B_4H_4Se_2]$ was prepared as described in the literature.[17] The external reference for the ^{11}B NMR $[Bu_4N(B_3H_8)]$ was synthesized with the literature method.[51] Preparative thin-layer chromatography was performed with Merck 105554 TLC Silica gel 60 F_{254}, layer thickness 250 μm on aluminum sheets (20 × 20 cm). NMR spectra were recorded on a 400 and 500 MHz Bruker FT-NMR spectrometer. Residual solvent protons were used as a reference (δ, ppm, $[D_8]$toluene, 2.09), while a sealed tube containing $[Bu_4N(B_3H_8)]$ in $[D_6]$benzene (δ_B, ppm, −30.07) was used as an external reference for the ^{11}B NMR. Infrared spectra were recorded on a Nicolet 6700 FT spectrometer. Mass spectra were obtained on a Jeol SX 102/Da-600 mass spectrometer with argon/xenon (6kv, 10 mÅ) as FAB gas. CH analyses were obtained on a Flash EA series 1112 CHNS analyzer.

Synthesis of 2. To a 100 mL Schlenk tube containing $[Cp^*TaCl_4]$ (0.16 g, 0.35 mmol) suspended in toluene (15 mL) and cooled to −78 °C, $[LiBH_4\cdot THF]$ (1.7 mL, 3.49 mmol) was added via syringe, and the reaction mixture was warmed slowly over 30 min to room temperature and left stirring for an additional hour. The solvent was evaporated under vacuum; the residue was extracted into hexane. The filtrate was concentrated, and a toluene solution (20 mL) of the intermediate was pyrolyzed in the presence of excess $[BH_3\cdot THF]$ (3.5 mL, 3.5 mmol) at 110 °C for 2 days. The solvent was dried, and the residue was extracted into hexane and passed through Celite. After removal of the solvent, the residue was subjected to a chromatographic work up using silica gel TLC plates. Elution with a hexane/CH_2Cl_2 (80:20 v/v) mixture yielded air stable yellow **2** (0.04 g, 16%), along with the other tantalaborane compounds reported earlier.[21] ^{11}B NMR ($[D_8]$toluene, 22 °C, 128 MHz): δ 23.9 (d, ^1J(H,B) = 135 Hz, 1B; BH), −0.8 (d, ^1J(H,B) = 123 Hz, 1B; BH), −4.3 (d, ^1J(H,B) = 120 Hz, 1B; BH), −34.1 (d, ^1J(H,B) = 125 Hz, 1B; BH). ^1H NMR ($[D_8]$toluene, 22 °C, 400 MHz): δ 6.13 (partially collapsed quartet, pcq, $1BH_t$), 5.64 (pcq, $1BH_t$), 2.22 (pcq, $1BH_t$), 2.17 (pcq, $1BH_t$), 2.10 (s, 30H; Cp*), −7.41 (br, 2Ta−H−B), −8.46 (br, 2Ta−H−B), −8.68 ppm (br, 2Ta−H−B). ^{13}C NMR ($[D_8]$toluene, 22 °C, 100 MHz): δ 110.4 (s; C_5Me_5), 11.4 (s; C_5Me_5). IR (hexane): 2438w (BH_t), 1380 (B−O). MS (FAB) P^+(max): m/z (%): 701. Elemental analysis (%) calcd for $C_{20}H_{40}B_4OTa_2$: C, 34.23; H, 5.75. Found: C, 34.05; H, 5.69.

Synthesis of 3 and 5. In a typical reaction, **2** (0.05 g, 0.07 mmol) in hexane (15 mL) was stirred with 3 equivalents of $[Fe_2(CO)_9]$ (0.07 g, 0.21 mmol) for 3 h at room temperature. The solvent was removed in vacuo; the residue was extracted in hexane and passed through Celite. The filtrate was concentrated and kept at −40 °C to remove $[Fe_3(CO)_{12}]$. The mother liquor was concentrated, and the residue was chromatographed on silica gel TLC plates. Elution with a hexane yielded a reddish brown **3** (0.04 g, 58%). In a similar fashion, reaction of **4** (0.06 g, 0.09 mmol) in hexane for 4 h at 70 °C provided reddish brown **5** (0.01 g, 8%) and cubane-type cluster $[(Cp^*Mo)_2(\mu_3\text{-}Se)_2B_2H(\mu\text{-}H)\text{-}\{Fe(CO)_2\}_2Fe(CO)_3]$ (0.014 g, 16%).[22]

dx.doi.org/10.1021/ic201046g |*Inorg. Chem.* 2011, 50, 9414–9422

Compound **3**: ^{11}B NMR ([D_8]toluene, 22 °C, 128 MHz): δ 153.3 (s, br, 1B), 27.9 (d, ^1J(H,B) = 126 Hz, 1B; BH), −10.0 ppm(d, ^1J(H,B) = 147 Hz, 1B; BH). ^{1}H NMR ([D_8]toluene, 22 °C, 400 MHz): δ 6.96 (pcq, 1BH$_t$), 4.13 (pcq, 1BH$_t$), 2.03 (s, 15H; Cp*), 1.84 (s, 15H; Cp*), −2.89 (br, 1Ta−H−B), −4.12 (br, 1 Ta−H−B), −7.93 (br, 1 Ta−H−B), −13.85 (s, 1 Ta−H−Fe), −16.54 ppm (s, 1 Ta−H−Fe). ^{13}C NMR ([D_8]toluene, 22 °C, 100 MHz): δ 214.0 and 212.7 (*C*O), 112.1 and 110.8 (s; C_5Me_5), 11.0 and 10.6 (s; $C_5\mathit{Me}_5$). IR (hexane): 2464w (BH$_t$), 2031, 1978, 1946 (Fe−CO), 1384 (B−O). MS (FAB) P$^+$(max): m/z (%): 967. Elemental analysis (%) calcd for $C_{26}H_{37}B_3O_7Fe_2Ta_2$: C, 32.27; H, 3.85. Found: C, 32.35; H, 3.87.

Compound **5**: ^{11}B{^{1}H} NMR (C_6D_6, 22 °C, 128 MHz): δ 162.5 (s, br, 1B), 158.2 (s, br, 1B), 106.2 (s, 1B), 67.8 ppm (s, br, 1B). ^{1}H NMR (C_6D_6, 22 °C, 400 MHz): δ 9.13 (pcq, 1BH$_t$), 1.86 (s, 15H; Cp*), 1.78 (s, 15H; Cp*), −15.65 ppm (br, 1Fe−H−B). ^{13}C NMR (C_6D_6, 22 °C, 100 MHz): δ 213.8 and 209.4 (*C*O), 108.8 and 107.3 (s; C_5Me_5), 12.1 and 11.9 (s; $C_5\mathit{Me}_5$). ^{77}Se NMR (C_6D_6, 22 °C): δ 954 (s, 1Se), 895 (s, 1Se). IR (hexane): 2464w (BH$_t$), 2012, 2001, 1976, 1957 (Fe−CO). MS (FAB) P$^+$(max): m/z (%): 1364. Elemental analysis (%) calcd for $C_{33}H_{32}B_4O_{13}Fe_6Mo_2Se_2$: C, 29.04; H, 2.36. Found: C, 28.92; H, 2.32.

X-ray Structure Determination. The Crystal data for **2** and **3** were collected and integrated using a Bruker Axs kappa apex2 CCD diffractometer, with graphite monochromated Mo−Kα (λ = 0.71073 Å) radiation at 293 K. Crystal data for **5** were collected and integrated using an Oxford Diffraction Xcalibur-S CCD system equipped with graphite-monochromated Mo−Kα radiation (λ = 0.71073 Å) at 150 K. The structures were solved by heavy atom methods using SHELXS-97[52] or SIR92[53] and refined using SHELXL-97.[54]

Crystal data for **2**: CCDC-739564. The hydrogen atoms attached to boron atoms were located by the difference Fourier map and were refined with the B−H distance constrained to 1.15 Å. The Cp* hydrogen atoms were fixed at geometrically meaningful positions and were given riding model refinement. All Cp* hydrogen atoms were placed in idealized locations; the four terminal and four bridging hydrogen atoms were located and refined. The two bridging hydrogen atoms were not located. Formula $C_{20}H_{40}B_4OTa_2$, M_r = 701.66 g/mol. Crystal system, space group: triclinic, $P\bar{1}$, a = 8.7520(4), b = 10.2507(4), c = 14.9209(5) Å, α = 71.0850(10), β = 77.089(2), γ = 73.679(2)°, Z = 2, ρ_{calcd} = 1.938 Mg/m^3. Final R indices [I > 2sigma (I)] R_1 = 0.0240, wR^2 = 0.0503. Index ranges −11 ≤ h ≤ 11, −13 ≤ k ≤ 13, −17 ≤ 1 ≤ 19, θ range for data collection 1.46 to 28.38°. Crystal size 0.25 × 0.22 × 0.19 mm. Reflections collected 16537, independent reflections 5865, [R (int) = 0.0228]. Goodness−of−fit on F^2 1.125.

Crystal data for **3**: CCDC-739565. The hydrogen atoms attached to boron atoms were located by the difference Fourier map and were refined with the B−H distance constrained to 1.1 Å. The Cp* hydrogen atoms were fixed at geometrically meaningful positions and were given riding model refinement. All Cp* hydrogen atoms were placed in idealized locations; the one terminal and three bridging hydrogen atoms were located and refined. The one terminal and two bridging hydrogen atoms were not located. Formula $C_{26}H_{37}B_3Fe_2O_7Ta_2$, M_r = 967.59 g/mol. Crystal system, space group: monoclinic, $P2_1/n$, a = 10.362(5), b = 8.747(5), c = 34.653(5) Å, β = 97.544(5)°, Z = 4, ρ_{calcd} = 2.066 Mg/m^3. Final R indices [I > 2sigma (I)] R_1 = 0.0440, wR^2 = 0.0884. Index ranges −15 ≤ h ≤ 15, −13 ≤ k ≤ 9, −51 ≤ 1 ≤ 41, θ range for data collection 1.19 to 32.29°. Crystal size 0.20 × 0.20 × 0.05 mm. Reflections collected 40277, independent reflections 10977, [R(int) = 0.0431]. Goodness-of-fit on F^2 1.100.

Crystal data for **5**: CCDC-769684. The hydrogen atoms attached to boron atoms were located by the difference Fourier map. The Cp* hydrogen atoms were fixed at geometrically meaningful positions and were given riding model refinement. All Cp* hydrogen atoms were placed in idealized locations; the one terminal B−H hydrogen atom was located and refined. The one bridging hydrogen atom was not located. Formula $C_{33}H_{32}B_4Fe_6Mo_2O_{13}Se_2$, M_r = 1364.73 g/mol. Crystal system, space group: monoclinic, $P2_1/n$, a = 13.6872(4), b = 18.8944(5), c = 16.9128(5) Å, β = 92.191(3)°, Z = 4, ρ_{calcd} = 2.145 Mg/m^3. Final R indices [I > 2sigma (I)] R_1 = 0.0385, wR^2 = 0.0828. Index ranges −16 ≤ h ≤ 13, −22 ≤ k ≤ 22, −20 ≤ 1 ≤ 20, θ range for data collection 3.35 to 25.00°. Crystal size 0.28 × 0.23 × 0.19 mm. Reflections collected 35721, independent reflections 7680, [R(int)=0.0737]. Goodness-of-fit on F^2 0.871.

Computational Methods. G09 suites of programs are used for Density Functional Theory studies.[55] Full molecular geometry optimization was performed by means of Becke's three parameter hybrid method using the LYP correlation functional (B3LYP), which combines the Hartree−Fock exchange term with the DFT exchange-correlation terms. The basis set employed are DGDZVP on H, B, C, O, and Se atoms and LANL2DZ on Fe, Mo, and Ta atoms. WBI and NBO methods are used to analyze the bonding patterns.

■ ASSOCIATED CONTENT

Supporting Information. Spectra for **2** and **3** and a combined X-ray crystallographic file for **2**, **3**, and **5** in CIF format; Wiberg bond indices (WBI) and *xyz* coordinates of the DFT optimized structures of compounds **2**, **3**, and **5**. This material is available free of charge via the Internet at http://pubs.acs.org.

■ AUTHOR INFORMATION

Corresponding Author
*E-mail: sghosh@iitm.ac.in.

■ ACKNOWLEDGMENT

Generous support of the Department of Science and Technology, DST (Project No. SR/S1/IC-19/2006), New Delhi is gratefully acknowledged. S.K.B. is grateful to the University Grants Commission (UGC), and K.G. thanks the Council of Scientific and Industrial Research (CSIR), India for research fellowships. K.H.K.R. would like to thank SERC and IISc for the computational facilities. We thank Shaikh M. Mobin for X-ray crystallography analysis. We would like to thank SAIF, IIT Madras for HSQC and variable temperature NMR.

■ REFERENCES

(1) Fehlner, T. P.; Halet, J.-F.; Saillard, J.-Y. *Molecular Clusters: A Bridge to Solid-State Chemistry*; Cambridge University Press: New York, 2007.

(2) Braunschweig, H. *Angew. Chem., Int. Ed.* **1998**, *37*, 1786–1801.

(3) (a) Greenwood, N. N.; Ward, I. M. *Chem. Soc. Rev.* **1974**, *3*, 231–271. (b) Grimes, R. N. *Acc. Chem. Res.* **1978**, *11*, 420–427. (c) Grimes, R. N. *Pure Appl. Chem.* **1982**, *54*, 43–58. (d) Grimes, R. N. In *Metal Interactions with Boron Clusters*; Grimes, R. N., Ed.; Plenum Publishing: New York, 1982; pp 269−319.

(4) (a) Kennedy, J. D. *Prog. Inorg. Chem.* **1984**, *32*, 519–670. (b) Kennedy, J. D. *Prog. Inorg. Chem.* **1986**, *34*, 211–434.

(5) (a) Barton, L.; Srivastava, D. K. In *Comprehensive Organometallic Chemistry II*; Wilkinson, G., Abel, E. W., Stone, F. G. A., Eds.; Pergamon Press: Elmsford, New York, 1995; Vol. 1, Chapter 8, pp 275−373. (b) Grimes, R. N. In *Comprehensive Organometallic Chemistry II*; Wilkinson, G., Abel, E. W., Stone, F. G. A., Eds.; Pergamon Press: Elmsford, New York, 1995; Vol 1, Chapter 9, pp 374−431.

(6) (a) Briguglio, J. J.; Sneddon, L. G. *Organometallics* **1985**, *4*, 721–726. (b) Kadlecek, D. E.; Carroll, P. J.; Sneddon, L. G. *J. Am. Chem. Soc.* **2000**, *122*, 10868–10877. (c) Jan, D.-Y.; Workman, D. P.; Hsu, L.-Y.; Krause, J. A.; Shore, S. G. *Inorg. Chem.* **1992**, *31*, 5123–5131.

(7) Meng, X.; Bandyopadhyay, A. K.; Fehlner, T. P.; Grevels, F.-W. *J. Organomet. Chem.* **1990**, *394*, 15–27.
(8) (a) Fehlner, T. P. *J. Chem. Soc., Dalton Trans.* **1998**, 1525–1531. (b) Fehlner, T. P. *Organometallics* **2000**, *19*, 2643–2651.
(9) Le Guennic, B.; Jiao, H.; Kahlal, S.; Saillard, J.-Y.; Halet, J.-F.; Ghosh, S.; Shang, M.; Beatty, A. M.; Rheingold, A. L.; Fehlner, T. P. *J. Am. Chem. Soc.* **2004**, *126*, 3203–3217.
(10) (a) Ghosh, S.; Beatty, A. M.; Fehlner, T. P. *Angew. Chem., Int. Ed.* **2003**, *42*, 4678–4680. (b) Ghosh, S.; Noll, B. C.; Fehlner, T. P. *Angew. Chem., Int. Ed.* **2005**, *44*, 2916–2918.
(11) Sahoo, S.; Dhayal, R. S.; Varghese, B.; Ghosh, S. *Organometallics* **2009**, *28*, 1586–1589.
(12) Ditzel, E. J.; Fontaine, X. L. R.; Fowkes, H.; Greenwood, N. N.; Kennedy, J. D.; MacKinnon, P.; Sisan, Z.; Thornton-Pett, M. *J. Chem. Soc., Chem. Commun.* **1990**, 1692–1694.
(13) Micciche, R. P.; Briguglio, J. J.; Sneddon, L. G. *Inorg. Chem.* **1984**, *23*, 3992–3999.
(14) Kim, Y.-H.; Brownless, A.; Cooke, P. A.; Greatrex, R.; Kennedy, J. D.; Thornton-Pett, M. *Inorg. Chem. Commun.* **1998**, *1*, 19–22.
(15) Frange, B.; Kennedy, J. D. *Main Group Met. Chem.* **1996**, *19*, 175.
(16) Bould, J.; Bown, M.; Kennedy, J. D. *Collect. Czech. Chem. Commun.* **2005**, *70*, 410–429.
(17) Sahoo, S.; Mobin, S. M.; Ghosh, S. *J. Organomet. Chem.* **2010**, *695*, 945–949.
(18) (a) Bose, S. K.; Geetharani, K.; Varghese, B.; Mobin, Sk. M.; Ghosh, S. *Chem.—Eur. J.* **2008**, *14*, 9058–9064. (b) Bose, S. K.; Geetharani, K.; Ramkumar, V.; Mobin, S. M.; Ghosh, S. *Chem.—Eur. J.* **2009**, *15*, 13483–13490.
(19) Fontaine, X. L. R.; Fowkes, H.; Greenwood, N. N.; Kennedy, J. D.; Thornton-Pett, M. *J. Chem. Soc., Chem. Commun.* **1985**, 1722–1723.
(20) (a) Housecroft, C. E. *Boranes and Metalloboranes*; Ellis Horwood: Chichester, U.K., 1990. (b) Shriver, D. F.; Kaesz, H. D. In *The Chemistry of Metal Cluster Complexes*; Adams, R. D., Ed.; VCH: New York, 1990.
(21) Ghosh, S.; Fehlner, T. P.; Noll, B. C. *Chem. Commun.* **2005**, 3080–3082.
(22) Geetharani, K.; Bose, S. K.; Sahoo, S.; Ghosh, S. *Angew. Chem., Int. Ed.* **2011**, *50*, 3908–3911.
(23) Galsworthy, J. R.; Housecroft, C. E.; Matthews, D. M.; Ostrander, R.; Rheingold, A. L. *J. Chem. Soc., Dalton Trans.* **1994**, 69–76.
(24) Wong, K. S.; Scheidt, W. R.; Fehlner, T. P. *J. Am. Chem. Soc.* **1982**, *104*, 1111–1113.
(25) Fehlner, T. P.; Housecroft, C. E.; Scheidt, W. R.; Wong, K. S. *Organometallics* **1983**, *2*, 825–833.
(26) Bandyopadhyay, A.; Shang, M.; Jun, C. S.; Fehlner, T. P. *Inorg. Chem.* **1994**, *33*, 3677–3684.
(27) (a) Housecroft, C. E. *Adv. Organomet. Chem.* **1991**, *33*, 1–50. (b) Housecroft, C. E. *Polyhedron* **1987**, *6*, 1935–1958. (c) Housecroft, C. E. *Coord. Chem. Rev.* **1995**, *143*, 297–330.
(28) (a) Hong, F.-E.; McCarthy, D. A.; White, J. P., III; Cottrell, C. E.; Shore, S. G. *Inorg. Chem.* **1990**, *29*, 2874–2876. (b) Housecroft, C. E.; Matthews, D. M.; Rheingold, A. L.; Song, X. *J. Chem. Soc., Dalton Trans.* **1992**, 2855–2864.
(29) Housecroft, C. E.; Matthews, D. M.; Rheinggold, A. L.; Song, X. *J. Chem. Soc., Chem. Commun.* **1992**, 842–843.
(30) Galsworthy, J. R.; Housecroft, C. E.; Rheingold, A. L. *J. Chem. Soc., Dalton Trans.* **1994**, 2359–2365.
(31) Jun, C. S.; Fehlner, T. P.; Rheingold, A. L. *J. Am. Chem. Soc.* **1993**, *115*, 4393–4394.
(32) Curtis, M. D.; Williams, P. D. *Inorg. Chem.* **1983**, *22*, 2661–2662.
(33) Bogan, L. E., Jr.; Rauchfuss, T. B.; Rheingold, A. L. *J. Am. Chem. Soc.* **1985**, *107*, 3843–3850.
(34) Richter, F.; Vahrenkamp, H. *Organometallics* **1982**, *1*, 756–757.
(35) Ogino, H.; Tobita, H.; Yanagisawa, K.; Shimoi, M.; Kabuto, C. *J. Am. Chem. Soc.* **1987**, *109*, 5847–5848.
(36) Zhang, Q.; Hong, M.; Liu, H. *Transition Met. Chem.* **1997**, *22*, 156–160.
(37) (a) Jemmis, E. D.; Balakrishnarajan, M. M.; Pancharatna, P. D. *J. Am. Chem. Soc.* **2001**, *123*, 4313–4323. (b) Jemmis, E. D.; Balakrishnarajan, M. M.; Pancharatna, P. D. *Chem. Rev.* **2002**, *102*, 93–144.
(38) Braunschweig, H.; Dewhurst, R. D.; Kraft, K.; Radacki, K. *Angew. Chem., Int. Ed.* **2009**, *48*, 5837–5840.
(39) Hong, F.-E.; Coffy, T. J.; McCarthy, D. A.; Shore, S. G. *Inorg. Chem.* **1989**, *28*, 3284–3285.
(40) Chung, J.-H.; Jordan, G.; Meyers, E. A.; Shore, S. G. *Inorg. Chem.* **2000**, *39*, 568–572.
(41) Khattar, R.; Puga, J.; Fehlner, T. P. *J. Am. Chem. Soc.* **1989**, *111*, 1877–1879.
(42) Bandyopadhyay, A.; Khattar, R.; Puga, J.; Fehlner, T. P.; Rheingold, A. L. *Inorg. Chem.* **1992**, *31*, 465–472.
(43) Bühl, M.; Schleyer, P. V. R. *J. Am. Chem. Soc.* **1992**, *114*, 477–491.
(44) Onak, T.; Tran, D.; Tseng, J.; Diaz, M.; Arias, J.; Herrera, S. *J. Am. Chem. Soc.* **1993**, *115*, 9210–9215.
(45) Fehlner, T. P. *Collect. Czech. Chem. Commun.* **1999**, *64*, 767–782.
(46) Wiberg, K. B. *Tetrahedron* **1968**, *24*, 1083–1096.
(47) Reed, A. E.; Curtiss, L. A.; Weinhold, F. *Chem. Rev.* **1988**, *88*, 899–926.
(48) Nagamatsu, J.; Nakagawa, N.; Muranaka, T.; Zenitani., Y.; Akimitsu, J. *Nature* **2001**, *410*, 63–64.
(49) Belashchenko, K. D.; van Schilfgaarde, M.; Antropov, V. P. *Phys. Rev. B* **2001**, *64*, 092503–092504.
(50) Messerle, L. *Chem. Rev.* **1988**, *88*, 1229–1254.
(51) Ryschkewitsch, G. E.; Nainan, K. C. *Inorg. Synth.* **1974**, *15*, 113–114.
(52) Sheldrick, G. M. *SHELXS-97*; University of Göttingen: Göttingen, Germany, 1997.
(53) Altonare, A.; Cascarano, G.; Giacovazzo, C.; Guagliardi, A. *J. Appl. Crystallogr.* **1993**, *26*, 343–350.
(54) Sheldrick, G. M. *SHELXL-97*; University of Göttingen: Göttingen, Germany, 1997.
(55) Frisch, M. J.; Trucks, G. W.; Schlegel, H. B.; Scuseria, G. E.; Robb, M. A.; Cheeseman, J. R.; Scalmani, G.; Barone, V.; Mennucci, B.; Petersson, G. A.; Nakatsuji, H.; Caricato, M.; Li, X.; Hratchian, H. P.; Izmaylov, A. F.; Bloino, J.; Zheng, G.; Sonnenberg, J. L.; Hada, M.; Ehara, M.; Toyota, K.; Fukuda, R.; Hasegawa, J.; Ishida, M.; Nakajima, T.; Honda, Y.; Kitao, O.; Nakai, H.; Vreven, T.; Montgomery, J. A., Jr.; Peralta, J. E.; Ogliaro, F.; Bearpark, M.; Heyd, J. J.; Brothers, E.; Kudin, K. N.; Staroverov, V. N.; Kobayashi, R.; Normand, J.; Raghavachari, K.; Rendell, A.; Burant, J. C.; Iyengar, S. S.; Tomasi, J.; Cossi, M.; Rega, N.; Millam, J. M.; Klene, M.; Knox, J. E.; Cross, J. B.; Bakken, V.; Adamo, C.; Jaramillo, J.; Gomperts, R.; Stratmann, R. E.; Yazyev, O.; Austin, A. J.; Cammi, R.; Pomelli, C.; Ochterski, J. W.; Martin, R. L.; Morokuma, K.; Zakrzewski, V. G.; Voth, G. A.; Salvador, P.; Dannenberg, J. J.; Dapprich, S.; Daniels, A. D.; Farkas, O.; Foresman, J. B.; Ortiz, J. V.; Cioslowski, J.; Fox, D. J. *Gaussian 09*, revision A.02; Gaussian, Inc.: Wallingford, CT, 2009.